JOURNAL OF CIVIL ENGINEERING AND MANAGEMENT
ISSN 1392-3730 print/ISSN 1822-3605 online
2011 Volume 17(3): 400–408
doi:10.3846/13923730.2011.594155

INVESTIGATION ON BEHAVIOUR OF SQUARE/RECTANGULAR REINFORCED CONCRETE COLUMNS RETROFITTED WITH FRP JACKET

Mohammad Hajsadeghi[1], Farshid Jandaghi Alaee[2], Amir Shahmohammadi[3]

[1, 2]*Department of Civil and Architectural Engineering, Shahrood University of Technology, 7th tir Square, Shahrood, Semnan, Iran*

[3]*School of Civil Engineering, University of Tehran, 16 Azar Street, Enghelab Ave, Tehran, Iran*

E-mails: [1]hajsadeghi_civil@yahoo.com (corresponding author); [2]fjalaee@shahroodut.ac.ir; [3]amir_shahmohammady@yahoo.com

Received 04 Aug. 2010; accepted 10 Nov. 2010

Abstract. The behaviour of fibre reinforced polymer (FRP)-wrapped concrete in circular columns has been extensively studied; however, much less is known about concrete in FRP-confined square/rectangular columns, in which the concrete is non-uniformly confined and the effectiveness of confinement is considerably reduced. This article presents the results of the numerical analysis of square/rectangular reinforced concrete (RC) columns confined with FRP jackets. Two prisms of size 250×250×500 mm and 150×300×500 mm were modelled and analysis was carried out using a non-linear finite element method. Two parameters of wrap thickness and fibre orientation were considered. The finite element analysis results were in good agreement with experimental data presented by other researchers. The numerical analysis results demonstrated significant enhancement in the compressive strength and ductility of the FRP-wrapped square/rectangular RC columns compared to unconfined RC columns. It was observed that the behaviour of the columns was greatly affected by the analysis parameters.

Keywords: FRP jacket, confinement, square/rectangular RC columns, finite element.

1. Introduction

Existing concrete structures may be found to perform unsatisfactorily for a variety of reasons. This could manifest itself by poor performance under service loading, in the form of excessive deflections and cracking, or there could be inadequate ultimate strength. Additionally, revisions in structural design and loading codes may render many structures previously thought to be satisfactory, noncompliant with current provisions. In the present economic climate, rehabilitation of damaged concrete structures to meet the more stringent limits on serviceability and ultimate strength of the current codes, and strengthening of existing concrete structures to carry higher permissible loads, seem to be a more attractive alternative to demolishing and rebuilding.

FRP materials as thin laminates or fabrics offer an ideal alternative for retrofitting of concrete structures. They generally have high strength to weight and stiffness to weight ratios and are chemically quite inert, offering significant potential for lightweight, cost effective and durable retrofit (Nanni 1995; Buyukozturk and Hearing 1998).

In recent years, FRP composites are used as externally bonded reinforcement to concrete structures for essentially two purposes: to provide confinement to concrete subjected to compression (jacketing system), and to improve bending and/or shear strength of a reinforced concrete flexural member such as beam, slab, etc. (Kamiński and Trapko 2006; Bulavs *et al.* 2005).

The carbon FRP (CFRP) composites, as unidirectional laminates, are ideal materials for confining existing concrete columns. When the FRP-wrapped concrete is subjected to an axial compression loading, the concrete core expands laterally. This expansion is resisted by the FRP; therefore the concrete core is changed to a three-dimensional compressive stress state. In this state, performance of the concrete core is significantly influenced by the confinement pressure. The confinement pressure provided by the FRP increases continuously with the lateral strain of concrete because of the linear elastic stress-strain behaviour of FRP, in contrast to steel-confined concrete in which the confining pressure remains constant when the steel is in plastic flow. Failure of FRP-wrapped concrete generally occurs when the hoop rupture strength of the FRP is reached (Mirmiran *et al.* 2000; Fam and Rizkalla 2001; Sadeghian *et al.* 2008).

2. Background

A number of studies have been conducted to investigate the confinement or jacketing effect of fibre reinforced polymer (FRP) wraps on the behaviour of concrete columns.

In a study by Parvin and Jamwal (2006), circular concrete columns were wrapped. Various parameters such as wrap thickness, fibre orientation, and concrete strength were studied. The results showed that the axial stress and axial strain carrying capacities of the wrapped concrete columns increased significantly as compared to the unconfined column and also, the behaviour of the columns was greatly affected by the analysis parameters. The behaviour of FRP-wrapped concrete cylinders with different wrapping materials and bonding dimensions has been studied by Lau and Zhou (2001) using the finite element method (FEM) and analytical methods. It was found that the load-carrying capacity of the wrapped concrete structure is governed by mechanical properties such as modulus and Poisson's ratio of the wrapping sheet. The technique of wrapping thin, flexible, and high-strength fibre composite straps around the column for seismic strengthening, to improve the confinement and thereby its ductility and strength has been presented by Saadatmanesh *et al.* (1994). The analytical compressive behaviour of concrete members reinforced with FRP was examined by Campione and Miraglia (2003), Youssef *et al.* (2007) and the variation in the shape of the cross-section was analysed. In a recent study, effect of corner radius on the performance of CFRP-confined square concrete columns has been studied by Wang and Wu (2008). The performance of wrapped concrete specimens subjected to severe environmental conditions such as wet, dry, and freeze-thaw cycles was investigated by Toutanji and Deng (2002). A study on the compressive behaviour and strength of elliptical concrete specimens wrapped with carbon fibre reinforced polymer (CFRP) has been described by Teng and Lam (2002). It was found by the study that the axial compressive strength of FRP-confined concrete in elliptical specimens is controlled by the amount of confining FRP and the major to minor axis length ratio of the column section. The behaviour of FRP-jacketed square concrete columns subjected to eccentric loading was studied by Parvin and Wang (2001). Mirmiran *et al.* (2000) focused on developing a non-linear FE model for the analysis of FRP-wrapped concrete. A parametric program was developed in ANSYS software to automatically generate the mesh for various geometric shapes and material properties. It was shown that the Drucker-Prager plasticity can be calibrated fairly well for predicting the axial stress-strain response. Doran *et al.* (2009) focused on developing a non-linear finite element modelling of square/rectangular concrete columns wrapped with FRP in order to simulate the compressive behaviour under concentric loading. Adopting cohesion and internal friction values of Drucker-Prager criterion from a previous study of the authors, emphasis is placed on both the determination of confining stress and the lateral-to-axial strain relation. Thirty three small and large scale specimens, including slender columns, tested by four different researchers are numerically analysed for this crucial relation between the behaviour of concrete and composite jacket. The distribution of confining stresses at the mid-height plane of the columns was evaluated on the basis of analysis. Confining stresses obtained from non-linear finite element analysis (NLFEA) were also compared with both uniform confining pressures for cylindrical specimens and effective stresses calculated by using a shape factor recommended by ACI 440.2R-02 (2002). Comparisons showed that the confining pressure values obtained from the assumption of uniform stress distribution over the surface of concrete core were consistent with the maximum lateral pressure at the corners while effective lateral pressure can be considered as minimum confining stresses on flat sides.

Considering the performed studies on FRP-wrapped concrete columns, it is evident that very limited data have been reported on square/rectangular columns retrofitted with FRP wrap, even though square/rectangular columns in need of a retrofit are very common.

The present study is a numerical investigation on FRP-wrapped square/rectangular RC columns. Two FRP-wrapped RC prisms were modelled and analysed by a non-linear finite element (FE) method and parameters of wrap thickness and fibre orientation were considered.

3. FE modelling of FRP-confined RC columns

In the present study a finite element model for square/rectangular RC columns confined with FRP composites is developed. The model is simulated using ANSYS 5.4 (1995) finite element software. The formulation of the FE model is discussed in the following sections.

3.1. Element types

The concrete core was modelled, using a special concrete element *SOLID65*. This element is an 8-noded solid brick element having three translation degrees of freedom per node (x, y, and z directions). This element has crushing (compressive) and cracking (tensile) capabilities. It is also capable of plastic deformation and creep.

SOLID45 element was used for the steel plates at the support and the loading areas as rigid bodies. The element is defined by eight nodes having three degrees of freedom at each node: translations in the nodal x, y, and z directions. The element has plasticity, creep, swelling, stress stiffening, large deflection, and large strain capabilities.

LINK8 element has been used to model the steel reinforcement (including longitudinal and transverse) in all the models. The element has two nodes. Each node has three-degrees of freedom, translations in the nodal x, y, and z directions. The element is also capable of plastic deformation.

The wrap was modelled by 4-noded linear elastic *SHELL41* element. *SHELL41* is a 3-D element having membrane (in-plane) stiffness but, no bending (out-of plane) stiffness. The element has three-degrees of freedom at each node: translations in the nodal x, y, and z directions. The element has variable thickness, stress stiffening, large deflection, and a cloth option. Cloth option is used for a tension-only behaviour. This non-linear option acts like a cloth in that tension loads will be supported but, compression loads will cause the element to wrinkle (ANSYS User's Manual revision 5.4 1995).

3.2. Material properties

3.2.1. Concrete

Development of a material model to represent the behaviour of concrete is a challenging task. Concrete is a quasi-brittle material and has different behaviour in compression and tension. In compression, the stress-strain curve for concrete is linearly elastic up to about 30% of the maximum compressive strength. Above this point, the stress increases gradually up to the maximum compressive strength. Once it reaches the maximum compressive strength (f'_c), the curve descends into a softening region, and eventually crushing failure occurs at an ultimate strain (ε_{cu}). In tension, the stress-strain curve for concrete is approximately linearly elastic up to the maximum tensile strength. After this point, the concrete cracks and the strength decreases gradually to zero. For concrete, ANSYS (ANSYS User's Manual revision 5.4 1995) requires material properties as follows: elastic modulus (E_c), uni-axial compressive strength (f'_c), uni-axial tensile strength (modulus of rupture, f_r), Poisson's ratio (υ_c), and shear transfer coefficient (β_t) as FE input data (for *SOLID65*). Elastic modulus and tensile strength of concrete is evaluated by following equations as per ACI 318M-08 (2010):

$$E_c = 4700\sqrt{f'_c}\ ; \tag{1}$$

$$f_r = 0.62\sqrt{f'_c}\ . \tag{2}$$

In this study, the cylindrical compressive strength of using concrete was 26.4 MPa and Poisson's ratio (υ_c) of concrete was assumed to be 0.2. The shear transfer coefficient (β_t) represents conditions of the crack face. β_t ranges from 0.0 to 1.0. β_t = 0 represents a smooth crack (complete loss of shear transfer) and 1.0 represents a rough crack (no loss of shear transfer).

Therefore, the shear transfer coefficient used in this study is 0.3 for a smooth crack and 0.99 for a rough crack. The ANSYS software also requires the non-linear behaviour of concrete in compression. Extensive experimental results have shown that the stress-strain curve of concrete uniformly confined with FRP features a monotonically ascending bi-linear shape (the increasing type) if the amount of FRP exceeds a certain value (Lam and Teng 2003; Mirmiran *et al.* 2000).

In this direction, the Drucker-Prager plasticity model was employed for modelling the non-linear behaviour of concrete in the tri-axial loading state, which assumes an elastic-perfectly plastic response (Mirmiran *et al.* 2000; Doran *et al.* 2009). The DP model is a smooth circular cone along the hydrostatic axis in principal stress space (Fig. 1). The DP cone for a tri-axial state of stress in concrete is defined as:

$$F = 3\beta\sigma_m + \sqrt{\frac{1}{2}}\{S\}^T[M]\{S\} - \sigma_y = 0\,, \tag{3}$$

where F is the yield function, σ_m is the hydrostatic stress, $\{S\}$ is the deviatoric stress, $[M]$ is a special diagonal matrix (Eq. 4), σ_y is the yield parameter of the material (Eq. 5), and β is a material parameter (Eq. 6). They are given by:

$$[M]_{6\times6} = \begin{bmatrix} I_{3\times3} & 0 \\ 0 & 2I_{3\times3} \end{bmatrix}, \tag{4}$$

$$\sigma_y = \frac{6C(\cos\phi)}{\sqrt{3}(3-\sin\phi)}\,, \tag{5}$$

$$\beta = \frac{2\sin\phi}{\sqrt{3}(3-\sin\phi)}\,, \tag{6}$$

where $I_{3\times3}$ is the indentity matrix, C is the cohesion of the material, φ is the internal friction angle of the material, and φ_f is dilatancy angle.

The large volumetric dilation of plain concrete does not occur until the peak strength is approached. This fact will be used in the DP model. A linearly elastic element will be combined with the DP criterion in an elastic-perfectly plastic element, where the yield level depends

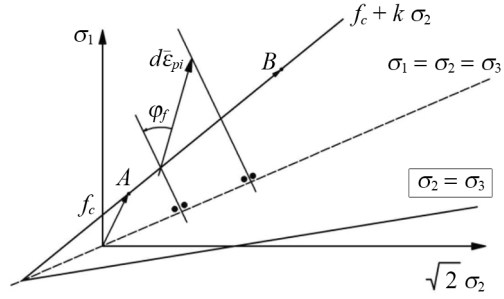

a) Plastic flow and failure surface

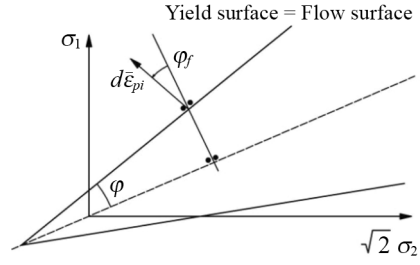

b) Associative flow rule

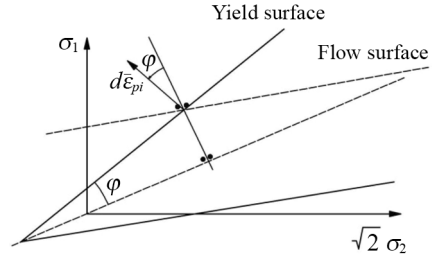

c) Non-associative flow rule

Fig. 1. Plastic flow and volumetric behaviour in Drucker-Prager (DP) model

on the level of confinement. Consider the plane where $\sigma_2 = \sigma_3$, shown in Fig. 1(a). Initially the element behaves perfectly linearly. At point A the strength capacity under the current confining stresses is reached. However, the DP criterion still allows for an increase in the strength increasing hydrostatic pressure, while plastic flow occurs on the failure surface. Plastic flow is controlled by a parameter φ_f, called the dilatancy angle. It determines the flow rule and the amount of volumetric straining during the occurrence of plastic flow. According to the plastic theory, the plastic strain increment vector $d\bar{\varepsilon}_{pl}$ is perpendicular to the flow surface at any point. If the flow surface and the yield surface are assumed the same, the flow rule is called associated and/or φ_f is equal to φ (Fig. 1(b)). If flow surface and yield surface are not coincident the flow rule is non-associated, as presented in Fig. 1(c). Placing $d\bar{\varepsilon}_{pl}$ in the 3D strain space, it can be seen that φ_f controls the volumetric behaviour.

In this research, input parameters values for defining the Drucker-Prager criteria (C: Cohesion, φ: Internal friction angle, φ_f: dilatancy angle) were calculated by equations presented by previous researchers (Mirmiran *et al.* 2000; Doran *et al.* 2009). With considering the relatively low precision of these values obtained from the equations and for best accordance of FE results with experimental data, a calibration analysis was conducted for models NS-R-1-200-3-40 and NS-R-2-175-3-40. This calibration analysis was carried out with considering three facts (Mirmiran *et al.* 2000):

1. The location of the transition point (point A) is a function of both cohesion and friction angle.
2. The second slope of the response depends mainly on the friction angle.
3. The best value of the dilatancy angle was determined as zero.

The adjusted values of cohesion, angle of internal friction, and dilatancy angle of concrete were selected to be 9.05 MPa, 15.0 degrees, and 0.0 degrees, respectively.

In the present study William-Warnke five-parameter failure model was used as failure criterion for concrete. Both cracking and crushing failure modes can be accounted for in it. The two input strength parameters, i.e., uniaxial tensile and compressive strengths, are needed to define a failure surface for the concrete. The most significant non-zero principal stresses are in the x and y directions and the mode of failure is a function of the sign of principal stress in the z direction. In a concrete element, cracking occurs when the principal tensile stress in any direction lies outside the failure surface. After cracking, the elastic modulus of the concrete element is set to zero in the direction parallel to the principal tensile stress direction. Crushing occurs when all principal stresses are compressive and lies outside the failure surface, subsequently, the elastic modulus is set to zero in all directions, and the contribution of element to stiffness matrix effectively reduces to zero. During this study, it was found that if the crushing capability of the concrete is turned on, the finite element models fail prematurely. Crushing of the concrete started to develop in elements located directly under the loads. Subsequently, adjacent concrete elements crushed within a few load steps as well, significantly reducing the local stiffness. Finally, the model showed a large displacement, and the solution diverged. Therefore, in this study, the crushing capability has been turned off and cracking of the concrete controlled the failure of the concrete elements.

3.2.2. Base plate and loading plate

The base and loading plates were modelled with the mechanical properties of steel (yield stress (f_y) and strain (ε_y) of the plates were 476 MPa and 0.0024).

3.2.3. Steel reinforcement

In this study, three types of steel reinforcing bars were used with diameters of 8 mm, 12 mm and 14 mm. the yield stress (f_y) and strain (ε_y) of the bars with diameters of 8 mm, 12 mm, 14 mm were 476 MPa and 0.0024, 339 MPa and 0.0017, and 345 MPa and 0.0017, respectively. The Poisson's ratio of the steel reinforcement (υ_s) was 0.3. In the finite element models, the steel has been assumed to be an elastic-perfectly plastic material and identical in tension and compression.

3.2.4. FRP

The FRP sheets are assumed as linear orthotropic materials. Therefore, four different material constants are to be given as input. The mechanical properties of the FRP that were used in this study are shown in Table 1.

Table 1. Mechanical properties of FRP sheets

Description	Coupon test data
Tensile modulus of elasticity	E_x = 230 GPa, E_y = 12 GPa
Shear modulus of elasticity	G_{xy} = 7 GPa
Poisson's ratio	υ_{xy} = 0.3
Tensile strength	f^*_{fu} = 3430 MPa
Ultimate rupture strain	ε_{fu} = 0.015
Nominal thickness	t_f = 0.165 mm/ply

3.3. Specimens geometry and specification

In this study, two prism specimens (columns) with dimensions of 250×250×500 mm and 150×300×500 mm were studied. The concrete cover and the corner's radius of specimens were 25 mm and 40 mm, respectively (see Fig. 2).

For square specimen, four 14 mm steel bars and for rectangular specimen, four 12 mm steel bars were used as longitudinal reinforcement, and for all specimens, six 8 mm stirrups were used as the transverse reinforcements. Each specimen was fully wrapped with one, three, or five uni-directional FRP layers in transverse direction. The specimen identification labels are presented in Table 2. The first letter in the label stands for square or rectangular cross section. The next character represents the number of FRP layers used to externally confine the specimens.

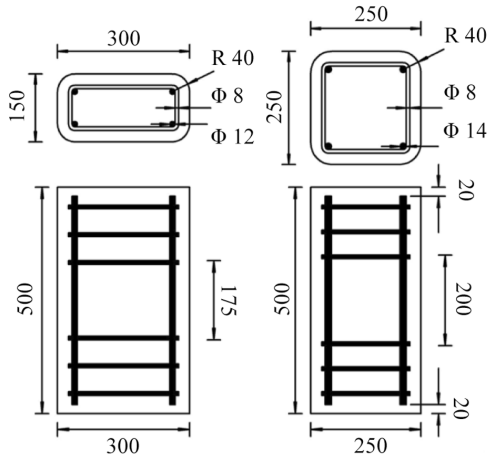

Fig. 2. Geometry of columns (Dimensions are in mm unit)

Table 2. Specimens specifications

Model ID	Cross section	Number of layers
S–1	Square	1
S–3	Square	3
S–5	Square	5
R–1	Rectangular	1
R–3	Rectangular	3
R–5	Rectangular	5

3.4. Boundary conditions, loading and solution

Due to the symmetry condition of the specimens, only a quarter of the specimens were modelled and the corresponding boundary conditions were applied to yz and zx planes (see Fig. 3). In order to simulate the steel plates at the ends of the models, two plates were modelled with the mechanical properties of steel, in those areas. Axial loading was applied on top surface of the loading plate using a user-defined loading increment. The axial load was applied to the top nodes of the loading plate and the bottom plate (base plate) was fixed from displacement in x, y, and z directions. Fig. 3 shows the finite element model of the rectangular specimens containing symmetric conditions.

Considering that FRP only resists tensile stresses, "tension-only" option of *SHELL41* was activated. In the finite element modelling of unconfined columns, with considering the small deformation of this type of columns, solution was selected to be linear in geometry. However, since it is expected to have large deformation in confined columns, the large displacement option was activated and the models were analysed as geometrical non-linear members.

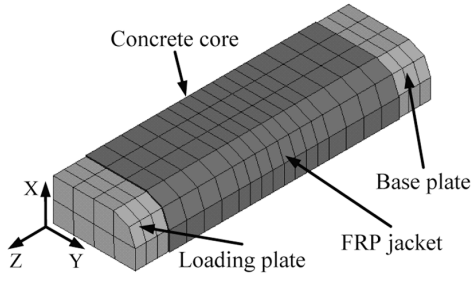

Fig. 3. FE modelling of 1/4 of rectangular specimens

The iterative Newton-Raphson procedure was used in the non-linear FE analysis. In this approach, the load (or displacement) is subdivided into a series of load (or displacement) increments. The load increments can be applied over several load steps. This follows an iterative procedure until the solution converges. A number of convergence enhancement features in ANSYS like automatic load stepping, line search, etc. can be activated to help the solution to converge. In the present analysis the automatic load stepping and the line search options were utilized. The automatic load stepping option allows ANSYS to determine the number of load steps required for an accurate solution. Sub-steps are defined to apply the loading, gradually. The number of sub-step used for the simulation varied from 100 to 200.

3.5. Failure criteria of specimens

The failure in the specimens occurs when the FRP fails. The maximum tensile strain observed in FRP wraps is usually lower than the value reported by manufacturers obtained from tensile coupon tests. Generally, premature failures are related to several parameters such as material stiffness, lay-up technique, and radius of curvature throughout the cross section. To avoid the overestimation of FRP strain capacities, a reduction factor of 48 percent was introduced to decrease the tensile rupture strain of FRP (Xiao and Wu 2000; Fam and Rizkalla 2001; Hajsadeghi and Alaee 2010). The failure in FRP was checked with the maximum strain failure criterion.

3.6. Mesh size effect

For evaluating mesh size effect of the models on the finite element results, a sensitive analysis on the mesh size was studied for specimen NS-R-2-175-3-40. The first model (with rough mesh) was meshed with 176 concrete elements (*SOLID65*) and the second (with fine mesh), with 2596 concrete elements (*SOLID65*). In Fig. 4, the specimen NS-R-2-175-3-40 with two mesh sizes is observed.

Fig. 5 shows a comparison between the stress-strain response of the FE models (models with rough and fine mesh) with experimental specimen. As it can be seen, the response of the model with fine mesh has a better accordance with experimental result; however, with considering the analysis time of these models (analysis time of the model with fine mesh is about 20 times of analysis time of the model with rough mesh) and the rational good result of the model with rough mesh, in the following modelling, this pattern of meshing was employed.

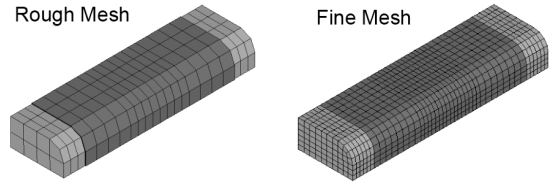

Fig. 4. Specimen NS-R-2-175-3-40 with two different mesh sizes (rough and fine mesh)

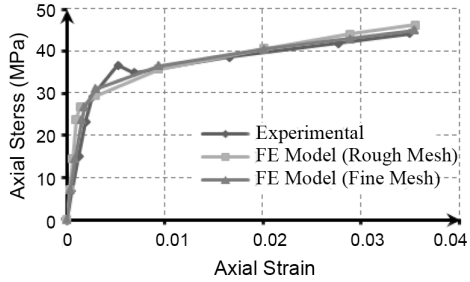

Fig. 5. The stress-strain responses of the FE models and experimental test (specimen NS-R-2-175-3-40

4. Results and discussion

4.1. Validation (comparison FE results with experimental data)

The validation of the FE analysis of the FRP-wrapped RC columns was checked with an experimental study reported by Ilki *et al.* (2008). Two specimens of NS-R-1-200-3-40 (square) and NS-R-2-175-3-40 (rectangular) were selected for the validation of the FE models. These specimens were the same as S–3 and R–3 in our FE models, respectively.

Fig. 6 shows a comparison between the stress-strain response of the control specimens obtained from the tests and that resulted from the FE analysis.

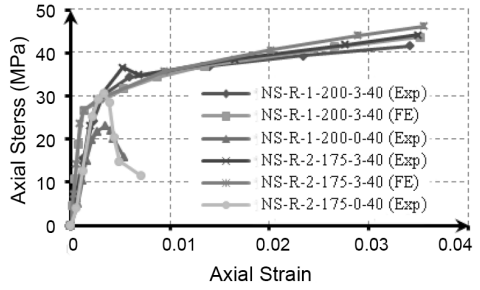

Fig. 6. Comparison of the stress-strain of the finite element modelling and experimental tests

For better understanding of the FRP jacket effect on the behaviour of the confined columns, the stress-strain responses of unconfined specimens (NS-R-1-200-0-40 and NS-R-2-175-0-40) are also shown in Fig. 6. In addition, the comparison of the finite element analysis (FEA) and the experimental results are presented in Table 3; in which f'_{cc} and ε_{ccu} are the maximum compressive stress and strain of the confined columns, respectively.

It can be seen that the FE analysis results are very close to the test results. This means that the FE model is valid for predicting the behaviour of specimens and can be used to conduct a parametric study.

Table 3. Comparison of the finite element modelling and experimental data

Specimens		NS-R-1-200-3-40		NS-R-2-175-3-40	
f'_{cc}	Exp	41.65	Dif.	44.2	Dif.
	FE	43.64	4.8%	46.2	4.5%
ε_{ccu}	Exp	0.0341	Dif.	0.0349	Dif.
	FE	0.0351	2.9%	0.0355	1.7%

4.2. Effect of wrap thickness

In this section, the effects of various wrap thicknesses on the behaviour of the FRP-wrapped RC columns are investigated.

To assess the confinement effect on the ductility of the specimens, the ductility ratios of all of the specimens were calculated. Ductility can be assessed by the ductility ratio, μ, which is defined by:

$$\mu = \frac{\text{Ultimate displacement}}{\text{Elastic displacement}}. \quad (7)$$

The ultimate displacement is defined as the point at which the load drops 20% from the peak load. The yield displacement is the yield point of an equivalent bi-linear response curve that provides an equal area to that of the response curve, as shown in Fig. 7. For specimens without a post-peak behaviour and for which the column failed at the peak point, the last point is used for the ultimate displacement (Wang and Wu 2008; Wu 2004).

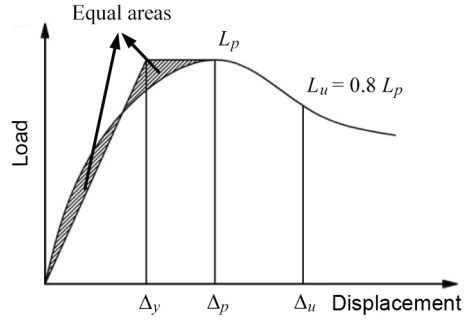

Fig. 7. Definition of ductility ratio

Fig. 8 and Fig. 9 show the stress-strain response of FE analysis results for the RC columns with three different wrap layers (one, three, and five). It is observed significant enhancement in the compressive strength and ductility of the columns compared to unconfined columns. With increasing of the number of layers, lateral confining pressure is increased. The increasing of the confining pressure causes that the concrete columns exhibit more axial stress and strain. Therefore, the columns with five layers exhibit the highest axial stress carrying capacity and axial strain (i.e. ductility) compared to other columns.

The ductility ratios of the specimens are provided in Table 4; also the increasing proportions of ductility ratio (confined specimens to unconfined specimens) are provided in it.

According to the Figs 8 and 9, the mean of load-carrying capacities of square and rectangular columns were increased 94% and 43%, respectively. Also according to the Table 4, the mean of ductility ratios of square and rectangular specimens are 7 and 8 times of ductility ratios of unconfined specimens, respectively.

Increasing of axial load-carrying capacity of the square specimens (because of wrapping the columns) is considerably higher than the rectangular specimens; however, they are not much different in increasing of ductility ratio.

As it was mentioned, in square/rectangular columns, concrete is non-uniformly confined. In Figs 10 and 11 the contours of compressive stress of concrete at mid-height of the square and rectangular columns are shown. As it can be seen, the stress distribution over these sections is non-uniform and the level of non-uniformity is increased with the increasing of the number of layers.

This phenomenon is caused by the shape of the cross section. In fact, at any location of the cross section different lateral pressure from FRP wrap is applied and therefore, the distribution of compressive stress becomes non-uniform. In all models, the maximum axial compressive stress occurs in the neighborhood of the corners and its minimum happens at the middle of the larger sides. Also it is evident that the square specimens in comparison with rectangular specimens have more effective area of cross section in carrying higher compressive stress (see Figs 10 and 11) that leads to the square specimens have more axial load-carrying capacities in comparison with the rectangular specimens.

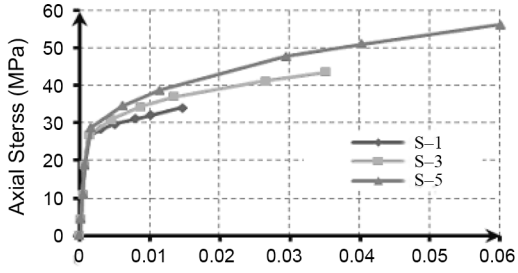

Fig. 8. Stress-strain curves of square RC columns

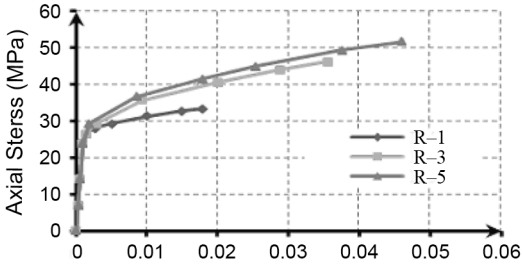

Fig. 9. Stress-strain curves of rectangular RC columns

Table 4. Ductility ratios

Ductility	Unconfined	Confined		Proportion
Square Specimens	1.8	S–1	5.50	3.06
		S–3	13.18	5.87
		S–5	22.51	12.13
Rectangular Specimens	1.54	R–1	6.72	4.36
		R–3	13.31	8.64
		R–5	17.25	11.20

The stresses around the perimeters of rectangular specimens are shown in Fig. 12. As observed, high corner stresses were noticeable for all specimens with low confinement stresses along the sides. As number of FRP layers increased, higher stress concentrations occurred at the corners. However, side confinement stresses did not increase as much due to lack of flexural rigidity of the FRP wrap. Thus, confinement stresses turned out to be more non-uniform as the layers of FRP wrap increased.

In Fig. 13 contour of strain for FRP jacket in hoop direction for specimen R–3 is shown. All column models wrapped with one, three, or five layers of FRP failed due to the rupture of FRP at near mid-height of the columns. Intensive stress concentration occurred at the corners where contact between concrete and FRP was the highest. This high outward contact force produced tensile strains in the FRP wrap in hoop direction.

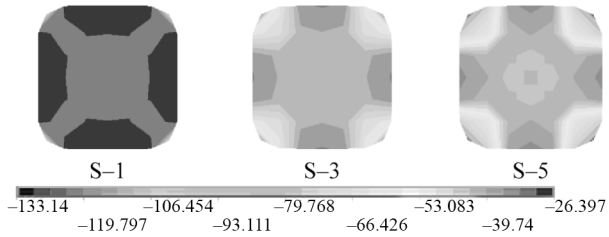

Fig. 10. Contours of axial compressive stress of concrete at mid-height of square columns

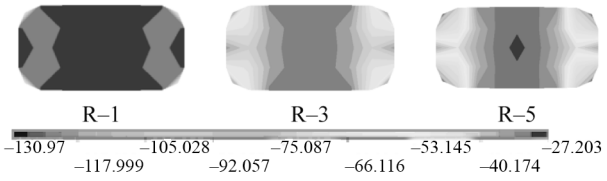

Fig. 11. Contours of axial compressive stress of concrete at mid-height of rectangular columns

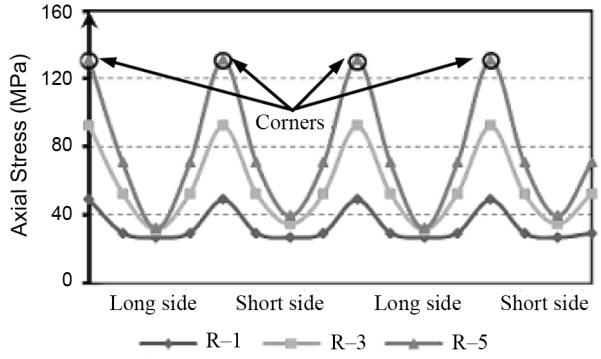

Fig. 12. FRP tensile strain distribution in specimen R–3

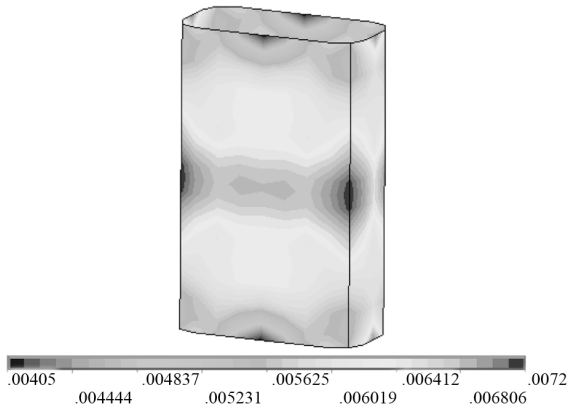

Fig. 13. FRP tensile strain distribution in specimen R–3

4.3. Effect of fibre orientation

In this section, the effect of fibre orientation of FRP jacket on the stress-strain response of specimens S–3 and R–3 is considered. The fibre orientation 0˚, ±15˚, ±30˚, and ±45˚ with respect to horizon were considered. Figs 14 and 15 show the effect of the fibre orientation on the stress-strain response of specimens S–3 and R–3, respectively.

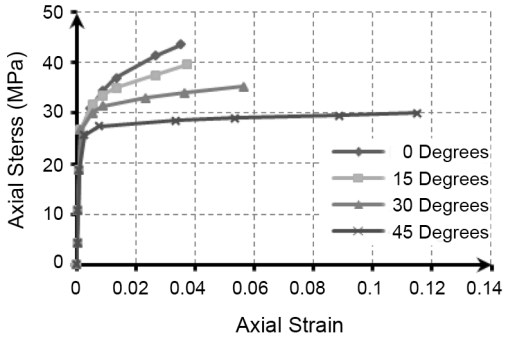

Fig. 14. Effect of fibre orientation on stress-strain response of specimen S–3

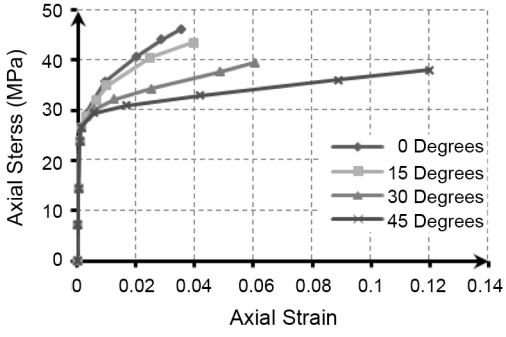

Fig. 15. Effect of fibre orientation on stress-strain response of specimen R–3

Table 5 shows ductility ratios of the specimens S–3 and R–3 versus the fibre orientation of the wrap.

It was observed that the fibre orientation of wrap strongly affects the stress-strain response of the specimens. It was also observed that the hoop orientation of fibres (0˚) results in the largest gain in ultimate stress, while the fibre orientation of ±45˚ leads to the largest ultimate strain (i.e. ductility). The specimen R–3 shows lower decreasing of axial load-carrying capacity in comparison with specimen S–3; however, they are not much different in increasing of axial strain and ductility.

When the fibre-wrapped concrete is subjected to an axial compression loading, due to bonding between concrete core and FRP jacket, FRP is deformed. In this case, considering the fibre orientation of wrap more than 0˚, the deformation causes the compression deformation of the fibres and leading FRP wrap fail with more lateral expanding concrete core. This phenomenon causes increasing the axial strain of specimens (i.e. ductility). However, fibre orientation (more than 0˚) leads to the applying less confining pressure to concrete core and concrete specimens exhibit less axial stress. The increasing of the fibre orientation causes that the concrete specimens exhibit more axial strain and less axial stress.

Table 5. Ductility ratios

Specimens	Fibre orientation			
	±0˚	±15˚	±30˚	±45˚
S–3	13.18	13.93	21.05	43.18
R–3	13.31	14.81	22.69	45.01

5. Conclusions

An efficient 3-D finite element model has been developed for the analysis of FRP wrapped square RC columns. The following conclusions can be drawn from this model:

1. The finite element analysis results showed substantial increase in the axial compressive strength and ductility of the FRP-wrapped RC columns compared with the unconfined columns.

2. The wrap thickness has a significant effect on the strength and ductility of the columns. Increasing the wrap thickness increases the strength and ductility of columns, considerably. Increasing of axial load-carrying capacity of the square specimens is significantly higher than that for rectangular specimens.

3. The study of axial stress contour in concrete at the mid-height for the columns shows that the strongest constraint zone is at the corner of the columns section and the weakest constraint appears at the middle of the sides.

4. The gain in axial compressive strength was observed to be the highest in the columns wrapped with the hoop orientation; but the highest axial strain and ductility were observed in the columns wrapped with the fibre orientation of ±45˚ with respect to the horizon. The rectangular specimen (R–3) shows lower decreasing of axial load-carrying capacity in comparison with square specimen (S–3); however, they are not much different in increasing of axial strain and ductility.

References

ACI 318M-08 Metric Building Code Requirements for Structural Concrete & Commentary. American Concrete Institute, 2010. 478 p.

ACI 440.2R-02 Guide for the Design and Construction of Externally Bonded FRP Systems for Strengthening Concrete Structures. ACI Committee 440, American Concrete Institute, 2002. 45 p.

ANSYS 1995. *User's manual revision 5.4*. Houston, PA. 56 p.

Bulavs, F.; Radinsh, I.; Tirans, N. 2005. Improvement of capacity in bending by the use of FRP layers on RC beams, *Journal of Civil Engineering and Management* 11(3): 169–174.

Buyukozturk, O.; Hearing, B. 1998. Failure behavior of precracked concrete beams with FRP, *Journal of Composites for Construction* 2(3): 138–144. doi:10.1061/(ASCE)1090-0268(1998)2:3(138)

Campione, G.; Miraglia, N. 2003. Strength and strain capacities of concrete compression members reinforced with FRP, *Cement and Concrete Composites* 25(1): 31–41. doi:10.1016/S0958-9465(01)00048-8

Doran, B.; Koksal, H. O.; Turgay, T. 2009. Nonlinear finite element modeling of rectangular/square concrete columns confined with FRP, *Materials & Design* 30(8): 3066–3075. doi:10.1016/j.matdes.2008.12.007

Fam, A. Z.; Rizkalla, S. H. 2001. Confinement model for axially loaded concrete confined by circular fiber-reinforced polymer tubes, *ACI Structural Journal* 98(4): 451–461.

Hajsadeghi, M.; Alaee, F. J. 2010. Numerical analysis of rectangular reinforced concrete columns confined with FRP jacket under eccentric loading, in *Proc. of the 5th International Conference on FRP Composites in Civil Engineering (CICE),* Beijing, China, 27–29 September, 2010. Paper 075: 658–661.

Ilki, A.; Peker, O.; Karamuk, E.; Demir, C.; Kumbasar, N. 2008. FRP retrofit of low and medium strength circular and rectangular reinforced concrete columns, *Journal of Materials in Civil Engineering* ASCE 20(2): 169–188. doi:10.1061/(ASCE)0899-1561(2008)20:2(169)

Kamiński, M.; Trapko, T. 2006. Experimental behaviour of reinforced concrete column models strengthened by CFRP materials, *Journal of Civil Engineering and Management* 12(2): 109–115.

Lam, M.; Teng, J. G. 2003. Design-oriented stress-strain model for FRP-confined concrete in rectangular columns, *Journal of Reinforced Plastics and Composites* 22(13): 1149–1186. doi:10.1177/0731684403035429

Lau, K.–T.; Zhou, L.–M. 2001. The mechanical behaviour of composite-wrapped concrete cylinders subjected to uniaxial compression load, *Composite Structures* 52(2): 189–198. doi:10.1016/S0263-8223(00)00167-7

Mirmiran, A.; Zagers, K.; Yuan, W. 2000. Nonlinear finite element modeling of concrete confined by fiber composites, *Finite Element in Analysis and Design* 35(1): 79–96. doi:10.1016/S0168-874X(99)00056-6

Nanni, A. 1995. Concrete repair with externally bonded FRP reinforcement: examples from Japan, *Concrete International* 97: 22–26.

Parvin, A.; Jamwal, A. S. 2006. Performance of externally FRP reinforced columns for changes in angle and thickness of the wrap and concrete strength, *Composite Structures* 73(4): 451–457. doi:10.1016/j.compstruct.2005.02.019

Parvin, A.; Wang, W. 2001. Behavior of FRP jacketed concrete columns under eccentric loading, *Journal of Composites for Construction* ASCE 5(3): 146–152. doi:10.1061/(ASCE)1090-0268(2001)5:3(146)

Saadatmanesh, H.; Ehsani, M. R.; Li, M. W. 1994. Strength and ductility of concrete columns externally reinforced with fibre composite straps, *ACI Structural Journal* 91(4): 434–447.

Sadeghian, P.; Rahai, A. R.; Ehsani, M. R. 2008. Numerical modeling of concrete cylinders confined with CFRP composites, *Journal of Reinforced Plastics and Composites* 27(12): 1309–1321. doi:10.1177/0731684407084212

Teng, J. G.; Lam, L. 2002. Compressive behaviour of carbon fibre reinforced polymer-confined concrete in elliptical columns, *Journal of Structural Engineering* 128(12): 1535–1543. doi:10.1061/(ASCE)0733-9445(2002)128:12(1535)

Toutanji, H.; Deng, Y. 2002. Strength and ductility performance of concrete axially loaded members confined with AFRP composite sheets, *Composites Part B: Engineering* 33(4): 255–261. doi:10.1016/S1359-8368(02)00016-1

Wang, L.-M.; Wu, Y.-F. 2008. Effect of corner radius on the performance of CFRP-confined square concrete columns: Test, *Engineering Structures* 30(2): 493–505. doi:10.1016/j.engstruct.2007.04.016

Wu, Y.-F. 2004. The effect of longitudinal reinforcement on the cyclic shear behaviour of glass fiber reinforced gypsum wall panels: tests, *Engineering Structures* 26(11): 1633–1646. doi:10.1016/j.engstruct.2004.06.009

Xiao, Y.; Wu, H. 2000. Compressive behavior of concrete confined by carbon fiber composites jackets, *Journal of Materials in Civil Engineering* ASCE 12(2): 139–146. doi:10.1061/(ASCE)0899-1561(2000)12:2(139)

Youssef, M. N.; Feng, M. Q.; Mosallam, A. S. 2007. Stress-strain model for concrete confined by FRP composites, *Composites Part B: Engineering* 38(5–6): 614–628. doi:10.1016/j.compositesb.2006.07.020

GELŽBETONINIŲ KVADRATINIO/STAČIAKAMPIO SKERSPJŪVIO FORMOS ELEMENTŲ, SUSTIPRINTŲ POLIMERINIU PLUOŠTU ARMUOTU APVALKALU, ELGSENOS TYRIMAS

M. Hajsadeghi, F. J. Alaee, A. Shahmohammadi

Santrauka

Apskritojo skerspjūvio armuotų betoninių elementų, sustiprintų polimeriniu pluoštu armuotu apvalkalu, elgsena yra išsamiai išnagrinėta. Daug mažiau žinoma apie tokių stačiakampio skerspjūvio elementų elgseną. Tokiuose elementuose betono deformacijos suvaržomos nevienodai, dėl to mažėja sustiprinimo efektyvumas. Straipsnyje pateikiami kvadratinio ir stačiakampio skerspjūvio gelžbetoninių elementų skaitinio tyrimo rezultatai. Taikant baigtinių elementų metodą buvo atlikta dviejų 250×250×500 mm ir 150×300×500 mm prizmių netiesinė analizė. Buvo išnagrinėta po du apvalkalo storio ir pluošto orientacijos atvejus. Baigtinių elementų analizės rezultatai gerai sutapo su eksperimentiniais kitų tyrėjų pateiktais duomenimis. Tyrimo rezultatai parodė, kad sustiprinimas žymiai padidina elementų gniuždomąjį stiprį ir stamantrumą, lyginant su analogiškais nesustiprintų elementų rodikliais. Buvo pastebėta, kad sustiprėjimo poveikis priklauso nuo apvalkalo rodiklių.

Reikšminiai žodžiai: polimeriniu pluoštu armuotas apvalkalas, sustiprinimas, kvadratinė/stačiakampė armuoto betoninė kolona, baigtiniai elementai.

Mohammad HAJSADEGHI. He received his Master of Science in structural engineering from Shahrood University of Technology (Iran) in 2009. His main research is behaviour of RC members and strengthening of concrete elements with FRP materials.

Farshid Jandaghi ALAEE. He received his Doctor of Philosophy from Cardiff University (UK) in 2002 and now he is an Assistant Professor at the Shahrood University of Technology (Iran). His major research interests are fibre reinforced polymer (FRP) for retrofitting, high-performance fibre-reinforced cement-based materials, and behaviour of reinforced concrete structures.

Amir SHAHMOHAMMADI. He received his Master of Science from University of Tehran (Iran) in 2009. His main research is strengthening of steel and reinforced concrete structures.